EJNMMI Research

ORIGINAL RESEARCH

Open Access

^{18}F-BMS-986229 PET imaging of tumor PD-L1 expression in glioblastoma patients

Milan Grkovski[1*], Mariza Daras[2], Tejus Bale[3], Serge Lyashchenko[4], Anne S. Reiner[5], Ingo K. Mellinghoff[6], Heiko Schöder[4] and Mark P. S. Dunphy[4*]

Abstract

Background Neurooncologists urgently need biomarkers that can optimize the clinical development of PD-L1 targeted immunotherapy in the treatment of glioblastoma. This study evaluated PD-L1 targeted tumor imaging by positron emission tomography (PET) in glioblastoma patients, using the novel macrocyclic peptide radiotracer ^{18}F-BMS-986229.

Results Twelve adult postsurgical glioblastoma patients underwent brain PET imaging 1-hour post injection 190±20 MBq of ^{18}F-BMS-986229. In a subset of patients, dynamic PET scans were obtained for pharmacokinetic modeling in tumors and normal tissues. Tracer kinetics in both tumor sites and normal tissues were well described by a reversible 1-tissue compartment model. Tumor sites demonstrated ^{18}F-BMS-986229 tracer-avidity (SUV = 1.1 ± 0.4; range, 0.6–1.7) in 10 of 12 cases, with negligible tracer-avidity in normal brain structures. Tumor avidity for ^{18}F-BMS-986229 on PET was spatially independent of tumor contrast-enhancement on magnetic resonance imaging, indicating that tracer-binding at tumor site was not dependent upon blood-brain barrier breakdown. The observed tumor site low tracer-uptake paralleled low immunohistochemical PD-L1 expression in resected tumors, with no correlations between standardized uptake value versus tumor MGMT methylation, PTEN oncogenic mutation status, tumor mutation burden, or patient overall survival.

Conclusion This pilot study demonstrates the feasibility of characterizing tumor sites in glioblastoma patients by PD-L1-targeted PET imaging with ^{18}F-BMS-986229, even in patients with low tumor PD-L1 expression. We hypothesize that ^{18}F-BMS-986229 PET can improve the pharmacometrics of PD-L1-targeted therapy trials.

Trial Registration Number NCT02617589. Trial Registration Date: December 1st, 2015.

Keywords ^{18}F-BMS-986229, PD-L1 expression, Glioblastoma, Pharmacokinetic modeling

*Correspondence:
Milan Grkovski
grkovskm@mskcc.org
Mark P. S. Dunphy
dunphym@mskcc.org
[1]Department of Medical Physics, Memorial Sloan Kettering Cancer Center, 1275 York Avenue, New York, NY 10065, USA
[2]Department of Neurology, Virginia Commonwealth University Health, Richmond, VA, USA
[3]Department of Pathology and Laboratory Medicine, Memorial Sloan Kettering Cancer Center, New York, NY, USA
[4]Molecular Imaging and Therapy Service, Department of Radiology, Memorial Sloan Kettering Cancer Center, 1275 York Avenue, New York, NY 10065, USA
[5]Department of Epidemiology-Biostatistics, Memorial Sloan Kettering Cancer Center, New York, NY, USA
[6]Department of Neurology, Memorial Sloan Kettering Cancer Center, New York, NY, USA

Introduction

Programmed death-ligand 1 (PD-L1) biomarkers are urgently sought to optimize ongoing clinical development of PD-L1 targeted cancer therapy [1, 2]. Tumor PD-L1 expression has demonstrated efficacy as a prognostic and predictive biomarker for PD-L1 targeted therapy in glioblastoma multiforme (GBM) and certain other cancer types [2, 3]. GBM PD-L1 expression is often low but might be increased, in vivo, by novel adjunct treatments, to improve GBM response rates to PD-L1 – directed immunotherapy [2]. Biopsy-based PD-L1 tumor assays are often impractical for brain tumor patients, being invasive, and are susceptible to inaccuracy due to tumor heterogeneity in PD-L1 expression [4–7]. Recently, PD-L1 targeted radiotracers havebeen-investigatedpreclinically [8–14] andintheclinicalsetting [3, 15–21] as a new class of intravenously-administered positronemission tomography(PET) imaging probes, showing promise for noninvasive quantification of in vivo tumor PD-L1expression. PET isapowerfulclinicalimagingtechniquethatenables noninvasive spatiotemporal assay of tissue binding of injected radiotracer to a biomolecular target of interest, with picomolar quantitative sensitivity. ^{18}F-BMS-986229 is an investigational macrocyclic peptide radiotracer (molecular weight 2296.63 Daltons) that binds to programmed death-ligand 1 (PD-L1, aka CD274). In this report, we describe the results of our phase 1/2 microdose PET pilot trial exploring PD-L1-targeted PET imaging with ^{18}F-BMS-986229 in postsurgical GBM patients. Our study demonstrates the feasibility of in vivo GBM detection via PD-L1 expression by ^{18}F-BMS-986229 PET. We explore correlations between tumor PD-L1 tracer-binding versus tumor histopathologic PD-L1expression, other biomarkers and patient survival.

Materials and methods

Patients

Newly diagnosed patients with GBM, O6-methylguanine-DNA-methyltransferase (MGMT) unmethylated type, and Karnofsky performance status of ≥70 were eligible for inclusion in this study. Radiopharmaceutical preparation is detailed in the Supplementary Materials. Patients received 190±20 MBq^{18}F-BMS-986229 by IV infusion over 1 min, followed by vigorous saline flush. Syringe and infusion line were assayed for residual activity. Patients were monitored for signs and symptoms of toxicity at each imaging time-point. Patients reported any adverse symptoms experienced in next 30 days to study investigators.

PET image acquisition

A single Discovery 710 PET-CT imaging system (GE Healthcare, Inc) was used for all patient studies. CT scans (120 kVp, 30 mAs, Pitch 0.984:1, reconstructed slice thickness 3.75 mm, 0.8 s per rotation) were acquired for attenuation correction and anatomic localization of PET data, spanning the entire brain. No intravenous radiographic contrast was administered. The CT data was reconstructed in a 512 × 512 matrix using a filtered back-projection algorithm. For three patients, dynamic PET imaging was performed: acquisition commenced twenty seconds prior to radiopharmaceutical infusion and continued for 2 h. Dynamic images were acquired in list mode and binned into 6 × 30-sec, 4 × 60-sec, 4 × 120-sec and 21 × 300-sec. For a subsequent cohort of nine additional patients, 30-min PET scans were obtained beginning 1-hr post-injection, acquired dynamically as a series of six five-minute frames, with PET data subsequently summed into a single static image. PET emission data were acquired in 3-dimensional mode, corrected for detector inhomogeneity, deadtime, decay, and for attenuation, scatter, and random events. The data were subsequently reconstructed into a 128 × 128 × 47 matrix (voxel dimensions: 2.00 × 2.00 × 3.27 mm^3) using the ordered subsets expectation maximization algorithm (4 iterations, 16 subsets). No post filtering was applied.

Image analysis

^{18}F-BMS-986229 brain PET-CT and brain magnetic resonance imaging (MRI) clinical scans were displayed for analytic comparison using an integrated GE PACS AW Suite workstation (GE Healthcare), using the Volume Viewer (v.12.3, GE Healthcare) software collection that included PET VCAR™, used for PET/CT fusion display, and Neuro Registration™, used for co-registration and display of PET with MRI data. Tissue tracer-avidity was quantified by standardized uptake values (SUV_{max} and SUV_{peak}) normalized to body weight, as measured from PET images by manual 3D volumes of interest (VOIs).

Pharmacokinetic modeling

The analysis of dynamic ^{18}F-BMS-986229 PET images was performed in PMOD v3.604 (PMOD Software, RRID: SCR_016547). Input function (IF) was image-derived by segmenting the internal carotid artery on the early frame that allowed for best visualization. To derive time-activity curves (TAC), VOIs were placed over the small intratumor area (≤10 voxels) with highest uptake of ^{18}F-BMS-986229, scalp (lateral and contralateral), site of craniotomy, pituitary gland and normal brain (contralateral). Reversible one-compartment (1C2K) and both irreversible and reversible two-tissue compartment (2C3K and 2C4K, respectively) pharmacokinetic models with a blood fraction component (v_B) were investigated to calculate kinetic rate constants K_1, k_2, k_3 and k_4. Target activity concentration at each time frame was weighed by considering frame duration and tissue activity concentration.

Goodness of fit was evaluated with Akaike Information Criterion (AIC) to determine the most appropriate compartmental model. In addition to pharmacokinetic modeling, Logan graphical analysis was performed to calculate the volume of distribution (V_T).

MRI image acquisition

MRI scans were obtained as part of routine clinical care using hardware and standard data acquisition and processing methods. MRI and ^{18}F-BMS-986229 PET images were obtained < 4weeks apart, with no interim changes in treatment. MRI was obtained using a 1.5 T magnet (Signa HDxt, GE Healthcare). Images were acquired using 5-mm slice thickness with no interslice gap (repetition time (TR) / echo time (TE) = 500/10 msec, matrix 256 × 256). Gadopentetate dimeglumine (Magnevist, HealthCare Pharmaceuticals Inc.) was injected though a peripheral angiocatheter at a standard dose (0.2 mL/kg body weight, 40 mL, 2 cc/sec). Dynamic contrast-enhanced perfusion images with 3D postprocessing was performed in the MRI obtained contemporaneous with PET and/or follow-up subsequent MRI.

Immunohistochemistry (IHC) for PD-L1 expression in tumor tissue

PD-L1 expression was assessed by immunohistochemistry using a previously validated rabbit anti-human anti-PD-L1 monoclonal antibody. The streptavidin–biotin peroxidase complex method was utilized for immunohistochemical studies with antibody to PD-L1 antibody clone E1L3N (Cell Signaling Technology, Danvers, MA). Results were scored as the percentage of tumor cells with positive staining for PD-L1. Immunohistochemistry with PD-L1 E1L3N clone from Cell Signaling was clinically validated against PD-L1 22C3 (pharmDx) and found to be comparable [22].

Tumor mutational burden

Tumor mutation burden (TMB) was calculated using the total number of non-synonymous mutations divided by the total genomic target region for which mutations are reported. Clinical associations between high TMB and response to immune checkpoint inhibitors have been reported in several solid tumor types [23–27].

Statistics

Associations of categorical variables with the continuous variables SUV_{max} and SUV_{peak} were investigated with the Wilcoxon two-sample test. Correlation between continuous variables with SUV_{max} and SUV_{peak} were investigated with the Spearman rank correlation coefficient. The associations between SUV_{max} and SUV_{peak} with overall survival were investigated with Cox proportional hazards regression modeling. Follow-up time was calculated from date of PET to date of death for those who died or date of last follow-up for those who were censored. All tests were two-sided with an alpha level of statistical significance set at < 0.05. All statistical analyses were performed in SAS v9.4 (The SAS Institute, Cary, NC).

Results

Patients (n = 12; Table 1) experienced no adverse effects from the tracer injection. The study achieved the primary safety and feasibility endpoints. ^{18}F-BMS-986229 PET detected tracer-avidity at postsurgical brain tumor sites in 10 of 12 GBM patients. One of the two PET-negative patients had a technically suboptimal PET study. Tumor resection occurred 31 ± 6 (range 20–39) days prior to PD-L1 PET.

Post-resection tumor sites demonstrated relatively low tracer uptake (SUV = 1.1 ± 0.4 at 60 min post-injection; Table 2); however, as normal brain grey and white matter demonstrated negligible radiotracer uptake, tumor-to-background uptake ratio was visually distinct (Figs. 1, 2, 3 and 4). Tumor-to-normal brain ratios were 18.1 ± 10.1 (range, 8.0–44.4). Tumor-to-blood ratios at 90 min were 0.7 ± 0.2. The low avidity at tumor sites was consistent with ex vivo immunohistochemistry that overall detected low-to-nil tumor PD-L1 expression, as is common in GBM (Table 3). Three tumors (in 3 patients) had detectable PD-L1 by ex vivo IHC; of these, one patient had the highest observed tumor site SUV (patient #1; Fig. 1), one patient had minimal tumor site uptake after subtotal tumor resection (patient #7), and one patient had a suboptimal PET scan. We observed no statistical correlations between tumor site avidity for the PDL1-targeted tracer (SUV) versus tumor MGMT methylation, PTEN oncogenic mutation status, tumor mutation burden, or patient overall survival (Tables 4A, 4B and 5).

Tracer-avidity on PET and tissue enhancement on MRI demonstrated distinct spatial localizations in tumor site subregions, indicating tissue tracer-avidity was not a mere artifact of blood-brain barrier-breakdown. Tumor radiotracer-avidity on PET did not extend beyond the tumor region of signal abnormalities visualized by MRI. Some enhancing subregions did not demonstrate substantial tracer-avidity (Figs. 2 and 3). Within particular tumor sites, tracer uptake on PET was visualized in subregions of tissue contrast enhancement visualized by MRI but also in non-enhancing subregions (Fig. 4). The non-enhancing areas on MRI that demonstrate PET uptake may represent microscopic tumor cells and/or tumor-associated macrophages and microglia.

Dynamic PET data was performed for the first three patients (Table 6). Blood volume fraction was ≤ 13% in all investigated tissues (except for the pituitary gland), avoiding covariance with K_1 and k_2. The results from these initial acquisitions suggest simple static PET imaging might

Table 1 Cohort characteristics

Variable	Level	*N* (%)	Median
Sex	Male	7 (58)	
	Female	5 (42)	
SUV_{Max}	Continuous	11 (92)	1.27
SUV_{Peak}	Continuous	11 (92)	0.56
Visually positive	N	2 (17)	
	Y	10 (83)	
Pattern	Ill-defined	2 (17)	
	Shell*	8 (67)	
	N/A	2 (17)	
Extent of Resection	Gross tumor resection	4 (33)	
	Subtotal tumor resection	8 (67)	
PDL (clone E1L3N) expression (IHC)	Negative	7 (58)	
	0.02	2 (17)	
	0.03	1 (8)	
	Unable to get slides	2 (17)	
Tumor Mutation Burden (mt/Mb)	Continuous	10 (83)	4.4
PTEN Loss	PTENN48K (oncogenic)	1 (8)	
	PTENR130* nonsense/oncogenic	1 (8)	
	PTENR55Sfs*p (oncogenic frameshift insert)	1 (8)	
	PTENV53G missense mutation (non-oncogenic)	1 (8)	
	PTENX343_splice (oncogenic)	1 (8)	
	PTENY67del (non-oncogenic)	1 (8)	
	PTENY76* (oncogenic)	1 (8)	
	Wild type	3 (25)	
	Unable to assess	2 (17)	
MGMT Methylation	Methylated	6 (50)	
	Unmethylated	6 (50)	

*Layer of tracer-avidity confined to tumor periphery

Table 2 ^{18}F BMS-986229 biodistribution in brain tumors and cranial structures

	Time post-injection	
	60 min	90 min
Metric	**Avg ± SD (range)**	**Avg ± SD (range)**
Tumor SUV_{max}	1.0 ± 0.4 (0.6–1.7)	1.7 ± 1.2 (0.8–3.1)
Tumor SUV_{peak}	0.6 ± 0.3 (0.3–0.9)	0.9 ± 0.4 (0.5–1.2)
Blood SUV_{avg}	0.8 ± 0.2 (0.6–1.1)	0.8 ± 0.1 (0.8-1.0)
Normal brain SUV_{avg}	0.1 ± 0.0 (0.1–0.2)	0.1 ± 0.0 (0.1–0.1)
Choroid plexi SUV_{avg}	0.7 ± 0.2 (0.6-1.0)	0.6 ± 0.4 (0.3–1.1)
Bone SUV_{avg}	0.8 ± 0.4 (0.4–1.5)	0.9 ± 0.1 (0.8-1.0)
Muscle SUV_{avg}	0.9 ± 0.3 (0.5–1.3)	0.9 ± 0.3 (0.7–1.3)
Lacrimal gland SUV_{avg}	1.8 ± 0.6 (1.4–3.1)	1.9 ± 1.0 (0.8–2.6)
Pituitary SUV_{avg}	6.5 ± 1.7 (4.8–9.7)	5.2 ± 3.7 (3.0-9.5)

suffice to characterize tissue tracer-avidity. Static scans were therefore adopted for the remaining patients, in an attempt to simplify the protocol and minimize patient discomfort. ^{18}F-BMS-986229 tracer-concentrations in scalp tissue, inflamed craniotomy sites, and normal brain tissue achieved peak concentrations around 20 min post-injection, followed by tissue tracer-clearance (Fig. 3). Tumor tissues continued to accumulate radiotracer up to 2 h post-injection, suggesting delayed PET imaging will offer superior Tumor-to-Background image contrast. According to AIC, a simpler 1C2K model was generally preferred over 2C3K and 2C4K models (for the intra-tumor area with highest uptake, AIC was 288 ± 23 and 303 ± 23 for 1C2K and 2C3K models, respectively; $n = 3$ patients). Tumor tissue with the highest uptake of ^{18}F-BMS-986229 exhibited lower efflux (k_2) and higher V_T compared to normal scalp, site of craniotomy and normal brain. Spearman rank correlation coefficientρ between V_T and SUV in 18 investigated structures (6 per patient) was 0.86. Corresponding ρ between K_1-SUV and between k_2-SUV were 0.81 and − 0.71, respectively.

Intracranial areas of postsurgical dural / parenchymal inflammation demonstrated transient tracer influx with prompt efflux (Fig. 2), consistent with nonspecific tracer extravasation due to capillary leakiness typical of tissue inflammation. In contrast, pharmacokinetics in the initial 3 patients identified a rise and plateau in tumor site SUV, consistent with true tumor site-binding of the PD-L1-targeted ^{18}F BMS-986229 tracer. The observed plateau in radiotracer concentration at tumor sites indicates that a simpler static PET scan at a delayed time-point is appropriate for characterizing tumor site avidity for ^{18}F BMS-986229, with high target-to-background contrast.

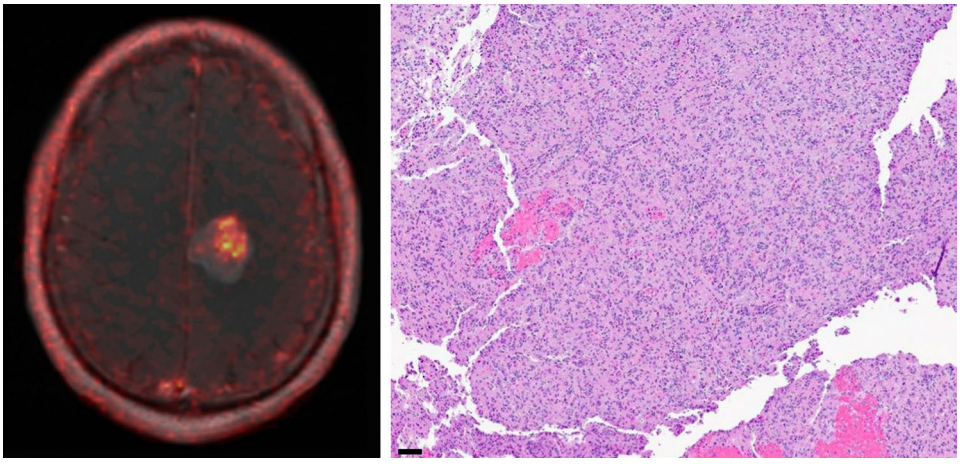

Fig. 1 68 year old male [Patient #1]. MRI (left) shows blood products within resection cavity and enhancing mural nodularity consistent with tumor which demonstrates avidity for ^{18} F-BMS-986229. SUV display intensity scale (0.0-2.5). H&E sections (right) demonstrate malignant astrocytic cells with readily identifiable mitoses, consistent with glioblastoma. Scale bar (bottom left) = 100 µm

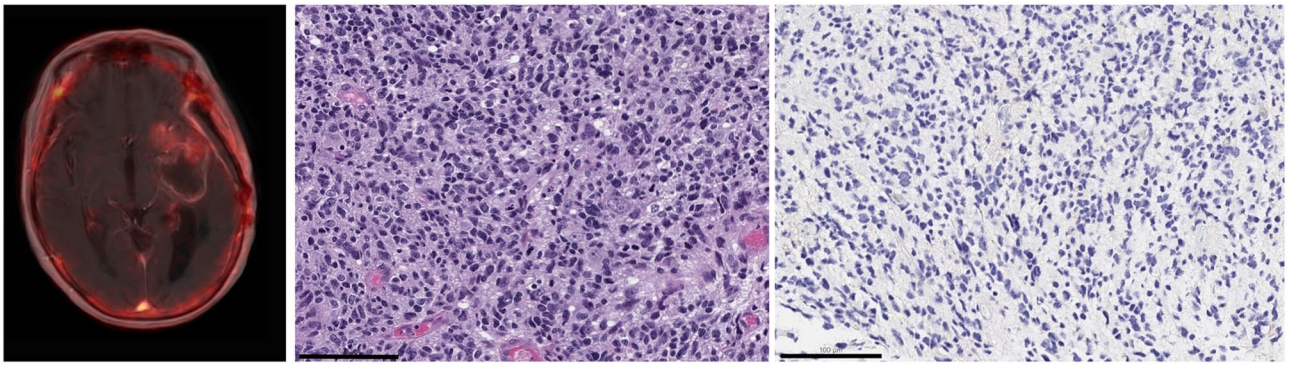

Fig. 2 72 year old female [Patient #8]. ^{18} F-BMS-986229 PET/MRI fusion (left) of a single axial plane focusing on tumor in the left cerebral hemisphere. MRI demonstrates uniform contrast-enhancement around surgical cavity. Nodular tissue enhancement along anterior margin of the cavity demonstrates prominent tracer-avidity, with minimal avidity in other enhancing tissues. Contrast-enhancing inflammation around craniotomy showed tracer-avidity. SUV display intensity scale (0.0-2.5). H&E sections (middle) demonstrate malignant astrocytic cells with readily identifiable mitoses, consistent with glioblastoma. Membranous labeling of tumor cells by PDL1 immunohistochemical stains was 0% (negative; right). Scale bar (bottom left) = 100 µm

Discussion

Our pilot study is, to best of our knowledge, the first report of ^{18}F-BMS-986229 PET, as well as of imaging tumor PD-L1 expression, in patients with GBM. We demonstrate the feasibility of detecting PD-L1 tracer-binding at postsurgical GBM tumor sites via same-day quantitative PET imaging. Negligible radiotracer accumulation in the normal brain enables high target-to-background ratios, increasing the contrast and lesion detectability. Tumor PD-L1 expression often predicts response to PD-L1 targeted pharmacotherapeutics (e.g., atezolizumab, durvalumab and avelumab) in various cancer types [28–30].

The patients were imaged ~ 1 month following initial tumor resection, as no delays in surgery and other treatment were tolerable. ^{18}F-BMS-986229 appears to bind to tumor sites with low-to-nil avidity; the patients in our cohort had low-to-nil ex vivo PD-L1 expression in their resected tumors (Table 3). Some patients with no detectable tumor PD-L1 expression ex vivo demonstrated low uptake by PET, possibly representing tracer-binding to infiltrates of inflammatory cells that can express PD-L1 [31]. Alternatively, low PET signal may reflect infiltrative tumor cells, potentially indicating early recurrence not visible on standard MRI. The highest observed tumor site radiotracer uptake occurred in one of three patients with detectable tumor PD-L1 expression and a subtotal resection. Two other patients had detectable tumor PD-L1 expression ex vivo: one had an aborted PET study (due to bladder urgency); the other patient had only minimal uptake following a gross total resection, similar to patients with no detectable tumor PD-L1 expression on ex vivo IHC.

Peptide-based imaging agents typically have restricted access to the central nervous system due to the selective nature of the blood-brain barrier (BBB). In pathological

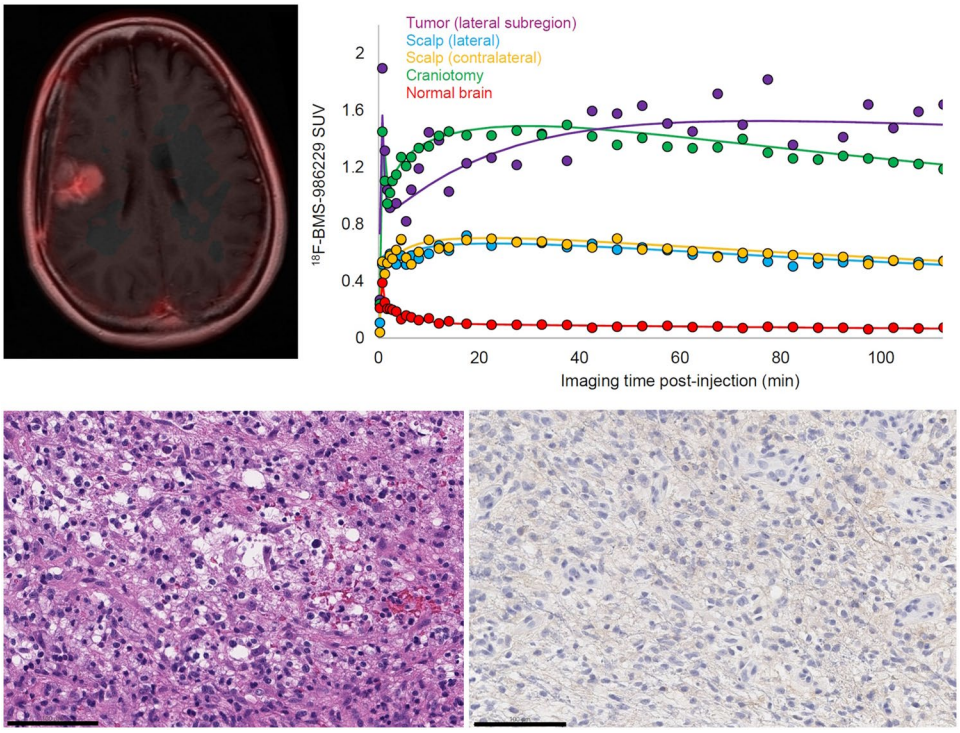

Fig. 3 57 year old F [Patient #2]. ^{18} F BMS-986229 PET/MRI fusion (top left) of a single axial plane showing tumor in right cerebral hemisphere. MRI demonstrates uniform contrast-enhancement in tumor. Lateral subregion of enhancing tumor demonstrates prominent tracer-avidity, with minimal avidity in remainder of enhancing tumor. SUV display intensity scale (0.0-2.5). Time-activity curves for structures of interest (top right). ^{18} F-BMS-986229 SUV as a function of imaging time post-injection for small intratumor area with higher uptake and for normal structures. Measured data (circles) are presented with fits from a 1-tissue reversible compartment model. H&E sections (bottom left) demonstrate malignant astrocytic cells with readily identifiable mitoses, consistent with glioblastoma. Membranous labeling of tumor cells by PDL1 immunohistochemical stains was 0% (negative; bottom right). Scale bar (bottom left) = 100 µm

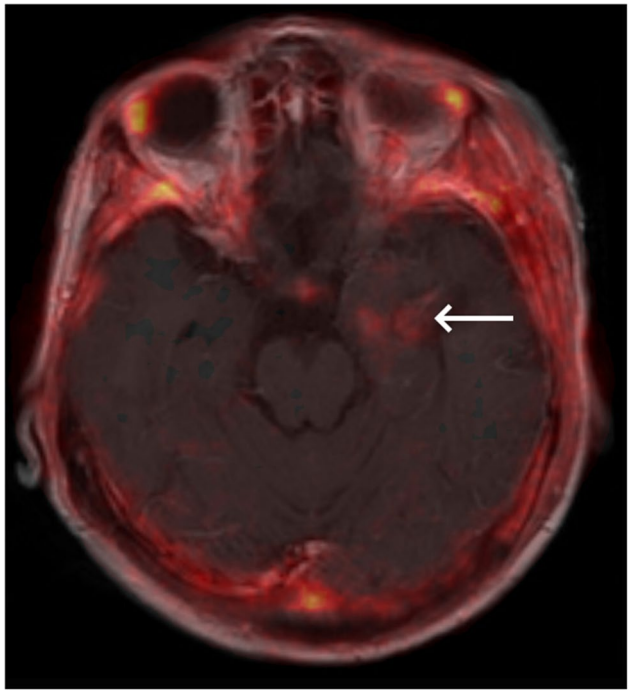

Fig. 4 69 year old female [Patient #10] with GBM status post resection with recurrent tumor (white arrow). ^{18} F BMS-986229 PET/MRI fusion. Radiotracer-avid tumor was non-enhancing on MRI. SUV display intensity scale (0.0-2.5)

conditions where the BBB is compromised—such as in certain brain tumors or metastases—there may be localized uptake of ^{18}F-BMS-986229. We observed no tracer-accumulation in healthy portions of the brains of our study population, where MRI visualized no abnormalities and the BBB is presumably intact. At brain tumor sites, even when no MRI contrast-enhancement is detectable, some degree of BBB breakdown is expected (^{18}F-BMS-986229 uptake was observed at tumor sites with no detectable MRI contrast-enhancement). As MRI contrast-enhancement correlates with BBB breakdown around tumors [32–35], the fact that we detected no correlation between the degree of contrast-enhancement on MRI and tracer-accumulation on PET suggests that tracer-accumulation in brain tumors was not solely a function of BBB breakdown.

Pharmacokinetic data indicates that ^{18}F-BMS-986229 tracer-kinetics are well described by a single tissue compartmental model. SUV appears to be an adequate surrogate measure of ^{18}F-BMS-986229 distribution volume, thus facilitating the use of simpler and clinically more feasible static PET acquisitions at a delayed time-point. This is in concordance with a report for another PD-L1 targeting investigational PET radiotracer ^{18}F-BMS-986,192 in patients with advanced non-small cell lung cancer [36].

Table 3 Patient-specific data regarding tumor avidity on PDL1-targeted PET, tumor histology, and treatment course

Pt#	Tumor SUV_{max}	Tumor SUV_{peak}	Visually detectable?	Ex vivo PDL1 expression (IHC) †	Extent of Resection	MGMT methylation	Dexamethasone dose (mg)†
1	3.11	1.24	Y	2%	STR	Methylated	4
2	1.35	0.99	Y	Negative	STR	Unmethylated	0
3*	0.24	0.10	N*	2%	STR	Unmethylated	4
4	0.78	0.54	Y	N/A	GTR	Unmethylated	4
5	0.64	0.30	N	Negative	GTR	Methylated	2
6	1.73	0.86	Y	Negative	STR	Unmethylated	4
7	0.82	0.36	Y	3%	GTR	Methylated	0
8	1.34	0.75	Y	Negative	STR	Unmethylated	3
9	0.88	0.40	Y	N/A	GTR	Methylated	0
10	0.89	0.46	Y	Negative	STR	Unmethylated	2
11	1.28	0.56	Y	Negative	STR	Methylated	N/A
12	1.27	0.57	Y	Negative	STR	Methylated	N/A

*PET was aborted prematurely. †PDL1 (clone E1L3N) expression. STR, subtotal resection. GTR, gross total resection. Slides were unavailable for patients #11 and #12

Table 4 Correlations between variables of interest and SUVmax

Variable	Level	SUV_{max} median	*P*-value
MGMT Methylation	Methylated	1.08	0.54
	Unmethylated	1.34	
PTEN Loss	Oncogenic Mutation	1.27	0.84
	Non-oncogenic mutation or WT	0.89	
Tumor mutation burden	continuous	Spearman's ρ: 0.04	0.91
Time from resection to PET	continuous	Spearman's ρ: 0.48	0.14

Table 5 Correlations between variables of interest and SUVpeak

Variable	Level	SUV_{peak} median	*P*-value
MGMT Methylation	Methylated	0.48	0.34
	Unmethylated	0.75	
PTEN Loss	Oncogenic Mutation	0.56	1.00
	Non-oncogenic mutation or WT	0.46	
Tumor mutation burden	Continuous	Spearman's ρ: 0.15	0.68
Time from resection to PET	Continuous	Spearman's ρ: 0.39	0.24

Additionally, plateau in ^{18}F-BMS-986229 tumor time-activity curves has also been reported in L2987 (PD-L1 (+)) mice by Donnelly et al. [18].

A limitation of this trial is the ability of ^{18}F-BMS-986229 PET to detect residual PD-L1 expressing tumor likely being hampered by low tumor volume in the postresection setting. We also did not obtain biopsies

Table 6 Association between SUV_{max} and overall survival

Variable	Level	HR	95% CI	*P*-value
SUV_{max}	Continuous	0.83	0.23–3.02	0.78
SUV_{peak}	Continuous	2.05	0.16–25.68	0.58

of the enhancing brain tissue at ~ 1 month post-resection, to correlate with the PET signal, due to potentially introducing considerable risk to the patients. Additionally, precise anatomical localization of the biopsied areas could not be accomplished as intraoperative imaging was not performed. In future studies, it would be most valuable to include PET imaging prior to initial surgery with anatomical localization of tissue samples, as well as postoperatively, during treatment with checkpoint blockade, and at disease progression. Such adequately powered studies might discover stronger correlations when comparing pre-surgical / pretreatment glioma tracer-avidity versus histology and outcome. Patients in our cohort had relatively low PD-L1 expression, confirmed by IHC and PD-L1 PET. GBM can demonstrate high PD-L1 expression [37], indicating the potential impact of this PD-L1 PET biomarker. Our pilot study was also limited in hypothesis-testing by its small study population, including our failure to detect correlations with patient outcomes. Four of the 12 patients that were imaged withdrew from the study prior to initiation of treatment, additional four patients came off the study relatively quickly due to disease progression and the remaining patients did not have a durable response to treatment. Immunohistochemistry studies have found PD-L1 expression prognostic in glioblastoma [37]; our patients went on to various treatments after participating in this research PET study, and certain treatments can alter tumor PD-L1

Table 7 Pharmacokinetic modeling of ^{18}F-BMS-986229 dynamic PET

	Tumor†	Scalp (lateral)	Scalp (contralateral)	Site of craniotomy	Normal brain (contralateral)	Pituitary gland
SUV*	1.29 ± 0.18	0.63 ± 0.11	0.68 ± 0.16	1.05 ± 0.19	0.08 ± 0.02	7.29 ± 1.12
V_B	0.13 ± 0.06	0.06 ± 0.04	0.06 ± 0.05	0.12 ± 0.08	0.04 ± 0.01	0.52 ± 0.14
K_1 (mL/min/g)	0.030 ± 0.013	0.024 ± 0.001	0.0025 ± 0.006	0.035 ± 0.019	0.007 ± 0.005	0.264 ± 0.095
k_2 (min^{-1})	0.027 ± 0.014	0.049 ± 0.014	0.047 ± 0.014	0.039 ± 0.017	0.166 ± 0.110	0.021 ± 0.006
V_T (mL/cc)	1.01 ± 0.17	0.61 ± 0.11	0.62 ± 0.09	0.63 ± 0.30	0.08 ± 0.02	6.58 ± 0.03

*averaged over last 30-min. V_T was derived from Logan graphical analysis

expression [2], potentially limiting correlations with outcomes.

Conclusions

We present first results of ^{18}F BMS-986229 PET in human glioblastoma patients, demonstrating its feasibility. The results encourage further clinical testing of PET radiopharmaceuticals as investigational biomarkers of in vivo tissue PD-L1 expression and as a companion diagnostic for PD-L1 targeted therapy.

Abbreviations

AIC	Akaike information criterion
GBM	glioblastoma multiforme
IF	input function
AIC	Akaike information criterion
IHC	Immunohistochemistry
MRI	Magnetic resonance imaging
PET	Positron emission tomography
SUV	Standardized uptake value
TAC	Time-activity curve
TMB	Tumor mutation burden

Acknowledgements

Not applicable.

Author contributions

MG - Design, PET image analysis, pharmacokinetic modeling, drafting the manuscript. MD - Conception and design, PET image analysis, drafting the manuscript. TB - Data analysis (immunohistochemistry, pathology), manuscript revision. SL - Radiopharmaceutical preparation, manuscript revision. ASR - Statistical analysis, manuscript revision. IKM - Conception and design, manuscript revision. HS - Conception and design, data acquisition, manuscript revision. MPSD - Conception and design, data acquisition, drafting the manuscript. All Authors have approved the submitted version and have agreed both to be personally accountable for the author's own contributions and to ensure that questions related to the accuracy or integrity of any part of the workare appropriately investigated, resolved, and the resolution documented in the literature.

Funding

This research was funded in part through the NIH/NCI Cancer Center Support Grant P30 CA008748 (PI: Selwyn M. Vickers).

Data availability

Data are available upon request.

Declarations

Ethics approval and consent to participate

This study was approved by the Institutional Review Board (Protocol #16–078, ClinicalTrials.gov Identifier: NCT02617589) and performed under an investigational new drug application approved by U.S. Food and Drug Administration. The analysis was conducted following the principles outlined in the Declaration of Helsinki. Patient clinical information was collected anonymously from electronic medical records.

Consent for publication

All patients provided written informed consent.

Competing interests

IKM reports receiving personal fees (advisory board services) from Agios, Black Diamond Therapeutics, Debiopharm Group, Erasca, Novartis, Prelude Therapeutics, Roche Therapeutics, Servier Pharmaceuticals, Voyager. IKM reports receiving grants from General Electric and Puma Biotechnology. No potential conflicts of interest relevant to this article exist.

Received: 4 April 2025 / Accepted: 6 July 2025
Published online: 26 September 2025

References

1. Iivanainen S, Koivunen JP. Possibilities of improving the clinical value of immune checkpoint inhibitor therapies in Cancer care by optimizing patient selection. Int J Mol Sci. 2020;21.
2. Tamura R, Tanaka T, Morimoto Y, et al. Alterations of the tumor microenvironment in glioblastoma following radiation and Temozolomide with or without bevacizumab. Ann Transl Med. 2020;8:297.
3. Bensch F, van der Veen EL, Lub-de Hooge MN, et al. (89)Zr-atezolizumab imaging as a non-invasive approach to assess clinical response to PD-L1 Blockade in cancer. Nat Med. 2018;24:1852–8.
4. Restrepo P, Yong R, Laface I et al. Tumoral and immune heterogeneity in an anti-PD-1-responsive glioblastoma: a case study. Cold Spring Harb Mol Case Stud. 2020;6.
5. Munari E, Zamboni G, Lunardi G, et al. PD-L1 expression heterogeneity in Non-Small cell lung cancer: defining criteria for harmonization between biopsy specimens and whole sections. J Thorac Oncol. 2018;13:1113–20.
6. Rasmussen JH, Lelkaitis G, Hakansson K, et al. Intratumor heterogeneity of PD-L1 expression in head and neck squamous cell carcinoma. Br J Cancer. 2019;120:1003–6.
7. Ben Dori S, Aizic A, Sabo E, Hershkovitz D. Spatial heterogeneity of PD-L1 expression and the risk for misclassification of PD-L1 immunohistochemistry in non-small cell lung cancer. Lung Cancer. 2020;147:91–8.
8. Lesniak WG, Chatterjee S, Gabrielson M, Lisok A, Wharram B, Pomper MG, Nimmagadda S. PD-L1 detection in tumors using [(64)Cu]Atezolizumab with PET. Bioconjug Chem. 2016;27:2103–10.
9. Chatterjee S, Lesniak WG, Nimmagadda S. Noninvasive imaging of immune checkpoint ligand PD-L1 in tumors and metastases for guiding immunotherapy. Mol Imaging. 2017;16:1536012117718459.
10. Truillet C, Oh HLJ, Yeo SP, et al. Imaging PD-L1 expression with ImmunoPET. Bioconjug Chem. 2018;29:96–103.
11. Jagoda EM, Vasalatiy O, Basuli F, et al. Immuno-PET imaging of the programmed cell Death-1 ligand (PD-L1) using a Zirconium-89 labeled therapeutic antibody, avelumab. Mol Imaging. 2019;18:1536012119829986.
12. Li M, Ehlerding EB, Jiang D, et al. In vivo characterization of PD-L1 expression in breast cancer by immuno-PET with (89)Zr-labeled avelumab. Am J Transl Res. 2020;12:1862–72.
13. Sharma G, Braga MC, Da Pieve C et al. Immuno-PET imaging of tumour PD-L1 expression in glioblastoma. Cancers (Basel). 2023;15.
14. Chevaleyre C, Zimmermann L, Specklin S et al. PET imaging of PD-L1 occupancy for preclinical assessment of the efficacy of combined Anti-PD-L1 immunotherapy and targeted therapy. J Nucl Med. 2025.
15. Vento J, Mulgaonkar A, Woolford L, et al. PD-L1 detection using (89)Zr-atezolizumab immuno-PET in renal cell carcinoma tumorgrafts from a patient with favorable nivolumab response. J Immunother Cancer. 2019;7:144.

16. Niemeijer AN, Leung D, Huisman MC, et al. Whole body PD-1 and PD-L1 positron emission tomography in patients with non-small-cell lung cancer. Nat Commun. 2018;9:4664.
17. Hegi-Johnson F, Rudd SE, Wichmann CW, et al. PD-L1 positron emission tomography imaging in patients with Non-Small cell lung cancer: preliminary results of the ImmunoPET phase 0 study. Int J Radiat Oncol Biol Phys. 2023;117:675–82.
18. Donnelly DJ, Kim J, Tran T, et al. The discovery and evaluation of [(18)F]BMS-986229, a novel macrocyclic peptide PET radioligand for the measurement of PD-L1 expression and in-vivo PD-L1 target engagement. Eur J Nucl Med Mol Imaging. 2024;51:978–90.
19. Cytryn SL, Pandit-Taskar N, Lumish MA, et al. (18)F-BMS-986229 PET to assess Programmed-Death ligand 1 status in gastroesophageal Cancer. J Nucl Med. 2024;65:722–7.
20. Badenhorst M, Windhorst AD, Beaino W. Navigating the landscape of PD-1/PD-L1 imaging tracers: from challenges to opportunities. Front Med (Lausanne). 2024;11:1401515.
21. Dar D, Rodak M, Da Pieve C, et al. Imaging PD-L1 in the brain-Journey from the lab to the clinic. Neuro Oncol. 2025;27:567–82.
22. Rimm DL, Han G, Taube JM, et al. A prospective, Multi-institutional, Pathologist-Based assessment of 4 immunohistochemistry assays for PD-L1 expression in Non-Small cell lung Cancer. JAMA Oncol. 2017;3:1051–8.
23. Snyder A, Makarov V, Merghoub T, et al. Genetic basis for clinical response to CTLA-4 Blockade in melanoma. N Engl J Med. 2014;371:2189–99.
24. Rizvi NA, Hellmann MD, Snyder A, et al. Cancer immunology. Mutational landscape determines sensitivity to PD-1 Blockade in non-small cell lung cancer. Science. 2015;348:124–8.
25. Van Allen EM, Miao D, Schilling B, et al. Genomic correlates of response to CTLA-4 Blockade in metastatic melanoma. Science. 2015;350:207–11.
26. Goodman AM, Kato S, Bazhenova L, et al. Tumor mutational burden as an independent predictor of response to immunotherapy in diverse cancers. Mol Cancer Ther. 2017;16:2598–608.
27. Le DT, Durham JN, Smith KN, et al. Mismatch repair deficiency predicts response of solid tumors to PD-1 Blockade. Science. 2017;357:409–13.
28. Stutvoet TS, van der Veen EL, Kol A et al. Molecular imaging of PD-L1 expression and dynamics with the adnectin-based PET tracer (18)F-BMS-986192. J Nucl Med. 2020.
29. Herbst RS, Soria JC, Kowanetz M, et al. Predictive correlates of response to the anti-PD-L1 antibody MPDL3280A in cancer patients. Nature. 2014;515:563–7.
30. Carbognin L, Pilotto S, Milella M, et al. Differential activity of nivolumab, pembrolizumab and MPDL3280A according to the tumor expression of programmed Death-Ligand-1 (PD-L1): sensitivity analysis of trials in melanoma, lung and genitourinary cancers. PLoS ONE. 2015;10:e0130142.
31. Chauhan P, Lokensgard JR. Glial cell expression of PD-L1. Int J Mol Sci. 2019;20.
32. Holodny AI, Nusbaum AO, Festa S, Pronin IN, Lee HJ, Kalnin AJ. Correlation between the degree of contrast enhancement and the volume of peritumoral edema in meningiomas and malignant gliomas. Neuroradiology. 1999;41:820–5.
33. Pronin IN, Holodny AI, Petraikin AV. MRI of high-grade glial tumors: correlation between the degree of contrast enhancement and the volume of surrounding edema. Neuroradiology. 1997;39:348–50.
34. Bergamino M, Barletta L, Castellan L, Mancardi G, Roccatagliata L. Dynamic Contrast-Enhanced MRI in the study of brain tumors. Comparison between the extended Tofts-Kety model and a phenomenological universalities (PUN) algorithm. J Digit Imaging. 2015;28:748–54.
35. Hoffmann G, Preibisch C, Günther M, et al. Noninvasive blood-brain barrier integrity mapping in patients with high-grade glioma and metastasis by multi-echo time-encoded arterial spin labeling. Magn Reson Med. 2025;93:2086–98.
36. Huisman M, Niemeijer AL, Windhorst B et al. Quantification of PD-L1 expression with [(18)F]BMS-986192 PET/CT in patients with advanced stage non-small-cell lung cancer. J Nucl Med. 2020.
37. Hao C, Chen G, Zhao H, et al. PD-L1 expression in glioblastoma, the clinical and prognostic significance: A systematic literature review and Meta-Analysis. Front Oncol. 2020;10:1015.

Publisher's note